PHYSICS AND CHEMISTRY OF SOLID STATE
V. 23, No. 4 (2022) pp. 741-755
Section: Chemistry

DOI: 10.15330/pcss.23.4.741-755

Vasyl Stefanyk Precarpathian National University

ФІЗИКА І ХІМІЯ ТВЕРДОГО ТІЛА
Т. 23, № 4 (2022) С. 741-755
Хімічні науки

UDC: 544.47 ISSN 1729-4428

Ivan Mironyuk[1], Nazarii Danyliuk[2], Liliia Turovska[3], Ihor Mykytyn[1]

Structural, morphological and photocatalytic properties of TiO_2 obtained by thermolytic decomposition of the $[Ti(OH_2)_6]^{3+}•3Cl^-$ aquacomplex

[1]*Department of Chemistry, Vasyl Stefanyk Precarpathian National University, Ivano-Frankivsk, Ukraine, myrif555@gmail.com*
[2]*Educational and Scientific Center of Material Science and Nanotechnology, Vasyl Stefanyk Precarpathian National University, Ivano-Frankivsk, Ukraine, danyliuk.nazariy@gmail.com*
[3]*Department of Medical Informatics, Medical and Biological Physics, Ivano-Frankivsk National Medical University, Ivano-Frankivsk, Ukraine, lturovska@ifnmu.edu.ua*

Thermolytic decomposition in a chloride-acid medium of a titanium aquacomplex precursor solution $[Ti(OH_2)_6]^{3+}•3Cl^-$ as a result of its boiling at a temperature of (110-114) ^{0}C is accompanied by precursor hydrolysis and the formation of hydrate molecules $Ti(OH)_3Cl•2H_2O$, which, as a result of condensation, provide the formation of rutile TiO_2 with rod-shaped particles (30-80) nm long and (8-20) nm in diameter, combined into flower-shaped associates with a diameter of (200-280) nm. The specific surface of associates is 62 $m^2 \cdot g^{-1}$. IR spectroscopic studies of the precursor hydrolysis products and the synthesized oxide material show that the geometric parameters of TiO_5Cl octahedra of $Ti(OH)_3Cl$ $•2H_2O$ hydrate molecules are close to those of TiO_6 octahedra of TiO_2 rutile. The average Ti-O interatomic distance of octahedra of titanium-containing hydrate molecules is a kind of template that directs the process of TiO_2 crystallization towards the formation of rutile. Rutile TiO_2 nanopowder synthesized in this way is an effective photocatalyst for the photooxidation of organic dyes in an aqueous medium by ultraviolet radiation. The photocatalytic activity of the synthesized rutile TiO_2 was determined by neutralization of Congo Red (CR) dye dissolved in an aqueous medium. The effectiveness of TiO_2 was studied by examining the effect of TiO_2 amount and H_2O_2 concentration. It has been established that complete bleaching of the dye is achieved in just 10 minutes of UV irradiation at a photocatalyst concentration of 1.5 g/L, an H_2O_2 concentration of 5 mM, and an initial CR dye concentration of 5 mg/L, at reaction rate constant of 2.1959 min^{-1}.

Keywords: titania, rutile, Congo Red, photocatalyst.

Received 05 November 2022; Accepted 14 November 2022.

Introduction

In recent decades, environmental pollution has been one of the greatest problems of mankind. Wastewater treatment is one of the biggest responsibilities in developed countries. Huge amount of wastewater is generated daily with significant amounts of industrial pollutants, including organic dyes. To eliminate the environmental problem, scientists are developing the latest environmentally friendly nanoparticles to destroy such pollutants [1–3]. Currently, there are various methods for removing pollutants, such as precipitation, reverse osmosis, and adsorption [4,5], but there is one drawback – all these methods simply transfer pollutants from one phase to another, and do not completely destroy them. At the same time, the photocatalysis method shows great potential in water [6] and air purification, selective and ecological synthesis of organic compounds and hydrogen production [7], since it is available worldwide using solar energy [8] or UV irradiation [9]. Among the various existing photocatalysts, TiO_2 is the most widely studied and used in many applications due to its low cost, availability, and oxidative ability to degrade organic pollutants [10]. The main disadvantages of TiO_2 are a wide

band gap and a high rate of electron-hole recombination, which leads to a low quantum yield and low efficiency of photocatalytic reactions [11]. Therefore, today an important issue is the development of new methods for the synthesis of active TiO_2 for the destruction of organic pollutants from wastewater.

Titanium dioxide nanopowders having photocatalytic properties are preferably produced by the pyrolysis method. Thus, the authors of [12,13] obtained anatase TiO_2 by thermolytic decomposition of a mixture of titanium oxysulfate $TiOSO_4 \cdot H_2O$ and soda Na_2CO_3. At a synthesis temperature of (300-700) ^{0}C, an oxide material with particles of (20-50) nm in size is formed. The resulting titanium dioxide is effective in the photodegradation of organic pollutants in the aquatic environment by ultraviolet radiation.

A variation of the pyrolysis method is the synthesis of titanium dioxide by burning titanium compounds in a flame. To obtain aerodispersed TiO_2 in [14], the $TiCl_4$ vapor was burned in an oxygen-hydrogen flame at a temperature of (1400-1700) ^{0}C. Two main processes are carried out in the flame – the hydrolysis of titanium tetrachloride by water formed as a result of the combustion of hydrogen, and the condensation of $Ti(OH)_4 \cdot 2H_2O$ molecules. The general scheme for the formation of TiO_2 in a flame:

$$TiCl_4 + 2H_2O \rightarrow TiO_2 + 4HCl \qquad (1)$$

According to [14], by changing the concentration of $TiCl_4$ in the reaction of the mixture, it is possible to influence the particle size in the range from 15 to 30 nm. When changing the rate of the reaction flow, the oxygen content in it and, accordingly, the flame temperature, titanium dioxide is formed, in which the amount of the rutile phase varies from 20 to 60 wt.%. Anatase and rutile nanopowder mixtures synthesized in a flame exhibit photocatalytic activity in the oxidation of ammonia, organic dyes, destruction of microbial cells [14], oxidation of isopropanol in an aqueous medium [15], etc.

By thermocatalytic decomposition of titanium tetraisopropoxide $Ti(OC_3H_7)_4$ in toluene, the authors of [16] obtained nanopowder TiO_2, which, in terms of phase composition (80 wt.% anatase and 20 wt.% rutile) and particle size (20-50 nm), is close to industrial pyrogenic TiO_2 of the P25 brand of the German concern Evonik used as a reference material for comparing the performance of new titanium dioxide photocatalysts.

Researchers are looking for little-known titanium-containing compounds that, upon thermolytic decomposition, turn into titanium dioxide with special physical and chemical properties. To obtain rutile TiO_2 with particles in the form of flower-shaped associates, a chloride-acid solution of the $[Ti(OH_2)_6]^{3+} \cdot 3Cl^-$ aquacomplex was used as a precursor. Boiling a solution of this aquacomplex at a temperature of (110-114) ^{0}C leads to the formation of nanopowder rutile titanium dioxin with rod-shaped particles with a diameter of (8-20) nm and a length of (30-80) nm, which are combined into flower-shaped associates with a size of (140–280) nm. Flower-shaped TiO_2 exhibits high photocatalytic activity during the degradation of organic dyes in an aqueous medium by ultraviolet radiation.

Its photocatalytic activity exceeds that of Evonik's P25 titanium dioxide.

In this paper, the tasks were:

- to find out the course of chemical reactions, that, when $TiCl_4$ is combined with hydrochloric acid, lead to the formation of a titanium-containing aquacomplex $[Ti(OH_2)_6]^{3+} \cdot 3Cl^-$;
- to identify chemical processes that ensure the formation of TiO_2 nanoparticles in an acidic reaction medium;
- to study the structural and morphological characteristics of the synthesized titanium dioxide, to identify the factors that direct the crystallization process to the formation of single-phase rutile TiO_2;
- to study the photodegradation of the Congo Red dye solution by UV radiation with the participation of the synthesized TiO_2, as well as P25 titanium dioxide, to find out the effect of hydrogen peroxide H_2O_2 and a sample of TiO_2 on the course of photodegradation processes.

I. Experimental

1.1. Synthesis of TiO_2

The basic precursor for the liquid-phase synthesis of TiO_2 was a chloride-acid solution of the $[Ti(OH_2)_6]^{3+} \cdot 3Cl^-$ aquacomplex. For preparation, hydrochloric acid cooled to a temperature of (0÷-5) ^{0}C with a density of 1.170 g·cm^{-1} was mixed in small portions into titanium tetrachloride $TiCl_4$. The weight ratio between $TiCl_4$ and hydrochloric acid was 1.4:1.0. The temperature of the reaction medium when mixing the reagents did not exceed (15÷25) ^{0}C. The density of the resulting precursor solution at a temperature of 20 ^{0}C was 1.515 g·cm^{-1}. 50 ml of the precursor solution was poured into a glass beaker with a volume of 800 ml, and 250 ml of distilled water was added. A beaker with a dilute precursor solution was placed on an electric furnace and heated to a boiling point of 112 ^{0}C. During boiling, as the volume of the reaction medium decreased by no more than (15-20) %, due to the evaporation of water and HCl molecules, distilled water was added to the beaker and thus the initial volume of the solution was maintained. The process of boiling the reaction medium was carried out for 5 hours. At the final stage of this process, the boiling point of the reaction medium decreased to (106-108) ^{0}C. After (20-30) min from the start of boiling, the solution acquired a white color due to the formation of TiO_2.

It should be noted that the process of boiling the reaction medium is accompanied by intense acoustic cavitation. Gas bubbles that emerge from the volume of the boiling medium are destroyed and cause powerful hydraulic shocks directed into the volume of the reaction medium. Acoustic cavitation intensifies the course of both redox reactions and condensation processes in the reaction medium.

The synthesized TiO_2 nanoparticles are removed from the reaction medium by vacuum filtration. The removed product is washed with distilled water, dried for 2 hours at a temperature of 105 ^{0}C, and then calcined for 2 hours in an electric furnace at a temperature of 350 ^{0}C.

1.2. Characteristics of methods

X-ray phase analysis of the synthesized TiO_2 was carried out on a DRON-4-07 diffractometer in copper anode radiation. The beams were focused according to the Bragg-Brentano scheme.

TiO_2 particles were visualized using a transmission electron microscope, a JSM 2100F device. The acceleration voltage during operation of the device was 200 kV.

Infrared spectra (IR spectra) of titanium-containing hydrate molecules dissolved in hydrochloric acid and nanopowder TiO_2 were recorded on a SPECORD M80 spectrophotometer in the range of 300-4000 cm^{-1}. Samples for recording spectra were prepared by mixing a drop of hydrolysate (5 mg) or a sample of TiO_2 (4 mg) with dry KBr in a ratio of 1:100. The mixture was ground in a vibratory mill for 6 minutes. Transparent plates 20×5 mm^2 in size were formed from the prepared mixture by pressing.

The morphological characteristics of TiO_2, namely its specific surface area, pore volume, and pore size distribution, were calculated from N_2 adsorption/desorption isotherms. Adsorption studies were carried out at the boiling point of liquefied nitrogen (T = 77 K) on a Quantachrome Autosorb (Nova 2200e) automatic sorbometer. Before the study, the TiO_2 sample was calcined in vacuum at a temperature of 180 ^{0}C for 24 hours. The pore sire distributions (PSDs) were calculated using density functional theory (DFT) [17].

1.3. Photodegradation experiments

Photocatalytic experiments were carried out in a glass reactor with a working volume of 25 mL. The reactor was irradiated from two opposite sides with two 5W UV-LEDs; all the technical characteristics and operating principle of the microphotoreactor are described in detail in our previous articles [1]. UV-LEDs have a maximum emission at 365 nm. The reactor is equipped with an adjustable magnetic stirrer to ensure a stable and uniform suspension (water + catalyst). The organic Congo Red (CR) dye with a concentration of 5 mg/L was chosen as a model pollutant. The concentration of titanium photocatalyst was varied as follows: 0.5 g/L, 1.0 g/L and 1.5 g/L. For the rapid formation of hydroxyl radicals ($OH^{\cdot}$), a solution of hydrogen peroxide was added, changing the concentration: 0 mM, 0.5 mM, 2 mM, 5 mM. Kinetic curves were recorded automatically using a DT-1309 luxmeter; changes in the dye concentration were recorded without pre-sampling for analysis. The DT-1309 software allows you to record changes in illumination in the reactor using a computer. The method for recalculating the change in illumination in the reactor into the concentration of the dye is described in [1].

The mechanism of CR photodegradation kinetics was evaluated using the first-order kinetic equation of the Langmuir-Hinshelwood approximation, where the degradation rate depends on the number of dye molecules in solution [18]:

$$\ln\left(\frac{C_t}{C_0}\right) = -kt, \qquad (2)$$

where C_o is the initial concentration of CR, C_t is the concentration of CR in the solution at time t, k is the rate constant [19].

1.4. Experiment Design

Independent process variables that have a direct effect on the photoactivity of the synthesized samples were investigated using RSM (Response Surface Methodology). All calculations were performed using the Design Expert software (trial version V8.0.6). The variable process parameters were the concentration of the photocatalyst (0.5-1.5) g/L and the concentration of H_2O_2 (0-5) mM. To optimize the process, 12 experiments were carried out according to the main matrix of the experimental design shown in Table 1. The reaction rate constant of the CR photodegradation (Equation (9)) was chosen as the dependent variable. Table 1 shows the ranges and levels of the independent parameters A and B. The data of the proposed model were analyzed for reliability and suitability using analysis of variance (ANOVA). The experiments were carried out randomly to avoid system error. In RSM, the influence of two independent parameters was considered: the photocatalyst loading (A) and the concentration of H_2O_2 (B). Other reaction conditions, namely the concentration of CR (5 mg/L) and the volume of the solution (25 mL), were kept constant in all experiments.

Table 1

Independent parameters and their ranges.

Independent Parameters	Symbol	Level			
Photocatalyst loading (g/L)	A	0.5	1.0	1.5	
Concentration of H_2O_2 (mM)	B	0.0	0.5	2.0	5.0

II. Results and discussion

2.1. Chemical aspects of the formation of a titanium aquacomplex precursor

When chlorides of some transition metals are combined with hydrochloric acid, redox reactions occur. These reactions lead to a decrease in the charge of the metal cation by 1 and the attachment of water molecules and chlorine anions to it. According to the Brønsted-Lowry theory, hydrochloric acid is a mixture of H_3O^+ cations and Cl^- anions. In this mixture, hydroxonium cations H_3O^+ are strong acids conjugated with weak bases, Cl^- anions.

In particular, the $TiCl_4$ salt, when combined with hydrochloric acid, becomes a base and a neutralization reaction occurs between them. This reaction can be written as an equation:

$$TiCl_4 + 6H_3O^+ \rightarrow [Ti(OH_2)_6]^{3+} \cdot 3Cl^- + 6H^+ + \frac{1}{2}Cl_2 \qquad (3)$$

To form a titanium aquacomplex, one of the four Cl^- anions of the $TiCl_4$ molecule donates an electron to the Ti^{4+} cation, which turns into the Ti^{3+} cation, while atomic Cl attaches another Cl atom to itself and is removed from the reaction medium as a gaseous molecule.

From equation (3) we see that the hydroxonium cations H_3O^+ get rid of the proton, and the free H_2O molecules, as a strong acid, neutralize the molecules of the base $TiCl_3$. In the titanium aquacomplex, the $[Ti(OH_2)_6]^{3+}$ cation is an acid conjugated with a weak base, $3Cl^-$ anions.

2.2. Synthesis of TiO_2 in an acidic reaction medium

Synthesis of TiO_2 nanopowder as a result of thermolysis of $[Ti(OH_2)_6]^{3+}•3Cl^-$ solution is a special process, since it is carried out in a strongly acidic reaction medium (pH ~ 0.2-1.0). OH^- anions for the hydrolysis of Ti^{4+} cations are formed as a result of the reaction of the reduction of water molecules of the aquacomplex by electrons, with the participation of oxygen molecules absorbed by the medium according to the reaction:

$$2H_2O + O_2 + 4e^- \rightarrow 4(OH^-), \quad (4)$$

Electrons for this reaction are supplied by Ti^{3+} cations, which are oxidized when the precursor solution is heated:

$$Ti^{3+} \rightarrow Ti^{4+} + e^-, \quad (5)$$

as well as Cl^- anions oxidized during the destruction of the aquacomplex:

$$3Cl^- \rightarrow 1.5 \cdot Cl_2 + 3e^-, \quad (6)$$

The high acidity of the reaction medium limits the course of the hydrolysis of Ti^{4+} cations. Ti^{4+} cations add only three OH^- anions and, accordingly, one Cl^- anion each.

The formed $Ti(OH)_3Cl$ molecules add two more H_2O molecules each, forming $Ti(OH)_3Cl•2H_2O$ hydrate molecules. The general process of their formation is carried out according to the scheme

$$Ti^{4+} + 3(OH)^- + Cl^- + 2H_2O \rightarrow Ti(OH)_3Cl \cdot 2H_2O. \quad (7)$$

The structure of hydrate molecules is the TiO_5Cl octahedron.

During thermolytic process, due to the condensation of these molecules, TiO_2 nanoparticles of the rutile modification are formed:

$$Ti(OH)_3Cl \cdot 2H_2O \rightarrow TiO_2 + 3H_2O + HCl \quad (8)$$

The authors of [20], studying the solubility of $Ti(OH)_4$ in hydrochloric acid, found that $Ti(OH)_3Cl•2H_2O$ crystalline hydrate is formed in a saturated solution of titanium hydroxide, which is readily soluble in water and acetone.

We have found that the slow sublimation extraction of water from a solution of titanium aquacomplex $[Ti(OH_2)_6]^{3+}•3Cl^-$ at a temperature of (15-30) °C, by reducing the partial pressure of water vapor above the surface of the solution, due to its adsorption binding by silica gel, leads to the formation of a monolithic crystalline hydrate $Ti(OH)_3Cl•2H_2O$ within 30-40 days, which, when heated to a temperature of 300 ^{0}C, turns into TiO_2 nanoparticles of the rutile modification. The thermolytic decomposition of this crystalline hydrate and the structural and morphological properties of the resulting TiO_2 will be the subject of our separate publication. Fig. 1 shows the X-ray diffraction pattern of rutile TiO_2 obtained by boiling a solution of the titanium aquacomplex precursor $[Ti(OH_2)_6]^{3+}•3Cl^-$. The high intensity of the reflexes and the small width at half-height indicate a high degree of crystallinity of the oxide material.

The lattice parameters of rutile powder TiO_2 have the following values: $\alpha = 4.61720 \pm 0.00041$ Å, $c = 2.94965 \pm 0.00032$ Å.

The geometric characteristics of the TiO_6 octahedra of rod-shaped rutile (particle size 1-3×10-30 nm^2) and ellipsoid anatase (particle size 3.5×4.5 nm^2) determined in [21] show that the average Ti-O interatomic distance in rutile octahedra is 1.966, and in anatase octahedra, – 1.954 Å. In percentage terms, the average Ti-O bond length of the rutile phase is 0.6% higher than the average bond length of the anatase phase.

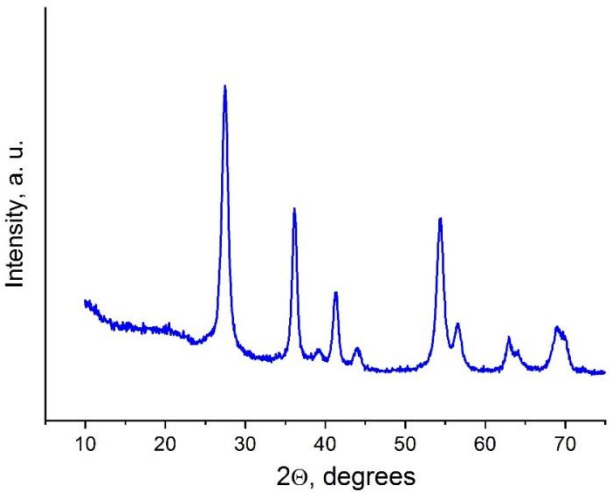

Fig. 1. X-ray diffraction pattern of rutile TiO_2 obtained using a titanium aquacomplex precursor.

Most likely, the average Ti-O bond length in $Ti(OH)_3Cl•2H_2O$ hydrate molecule is longer than the length of this bond in $Ti(OH)_4•2H_2O$ hydrate molecule, therefore, the geometric parameters of the octahedra of these molecules determine the formation of the TiO_2 crystal structure.

The liquid-phase sol-gel synthesis of TiO_2 using a solution of the $[Ti(OH_2)_6]^{3+}•3Cl^-$ aquacomplex precursor and NaOH hydrolyzing reagent leads to the formation of an anatase product [21]. The formation of the anatase phase in the course of this synthesis is carried out with the participation of $Ti(OH)_4•2H_2O$ molecules in the condensation process.

The average Ti-O interatomic distance in the octahedra of hydrate molecules $Ti(OH)_3Cl•2H_2O$ and $Ti(OH)_4•2H_2O$ is a kind of template reproduced during synthesis in rutile and anatase octahedra. To implement this scheme for the formation of TiO_2 crystalline phases, it is necessary, first, that the geometric parameters of the octahedra of $Ti(OH)_3Cl•2H_2O$ and $Ti(OH)_4•2H_2O$ molecules coincide with the parameters of the rutile and anatase octahedra, respectively, and, second, the average Ti-O distance in $Ti(OH)_3Cl•2H_2O$ molecules should be greater than in $Ti(OH)_4Cl•2H_2O$ molecules. The validity of these requirements can be confirmed by a comparative analysis of the IR spectra of titanium-containing hydrate molecules and TiO_2 crystalline phases.

2.3. Images of TiO_2 particles

The images of rutile TiO_2 obtained using a transmission electron microscope indicate that during liquid-phase synthesis, rod-shaped particles with a diameter of (8-20) nm and a length of (30-80) nm are formed, which are combined into flower-shaped associates with a diameter of (200-280) nm (Fig. 2-a); it is noteworthy that the sizes of associates are commensurate with the wavelengths of near ultraviolet radiation.

Particle images at 5 nm resolution (Fig. 2-b) allow the rows of atoms of the crystallographic planes to be seen. Measurements of interplanar distances showed that the crystallites are dominated by faces with indices (001) and (010). The area of these faces in the total specific surface area of powdered rutile is ~90%.

2.4. The porosity of associates

Adsorption/desorption isotherms of N_2 molecules by rutile TiO_2 are shown in Fig. 3-a. The parameters of the porous structure of the oxide material calculated from these isotherms are shown in Table 2, and the pore volume distribution by size is shown in Fig. 3-b.

Associates of rod-shaped particles contain mesopores ranging in size from 1 to 5 nm. Mesopores with a radius of ~2.3 nm predominate in the pore volume distribution by size. Mesopores in rutile TiO_2 are in fact gaps between rod-shaped particles in associates. The volume of

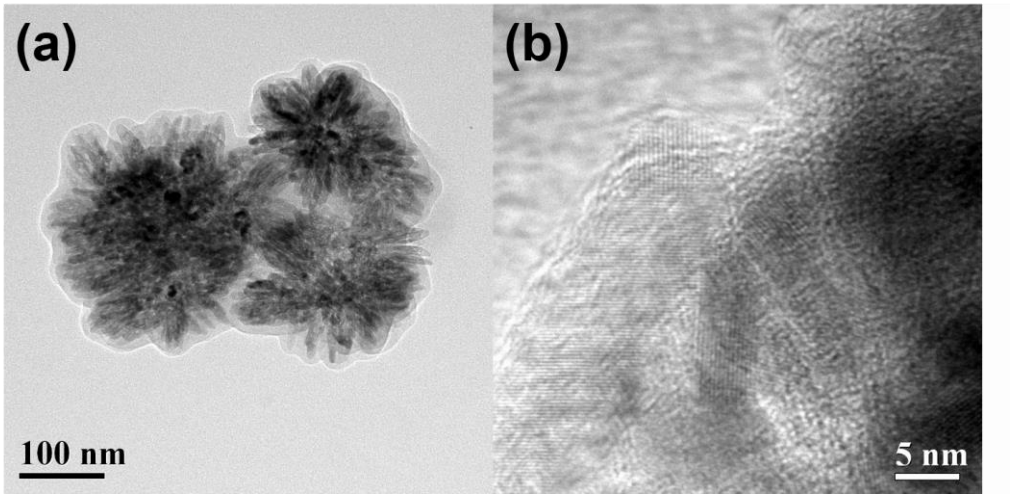

Fig. 2. Image of particles of rutile TiO_2: flower-shaped associates **(a)**; microcrystallite particles **(b)**.

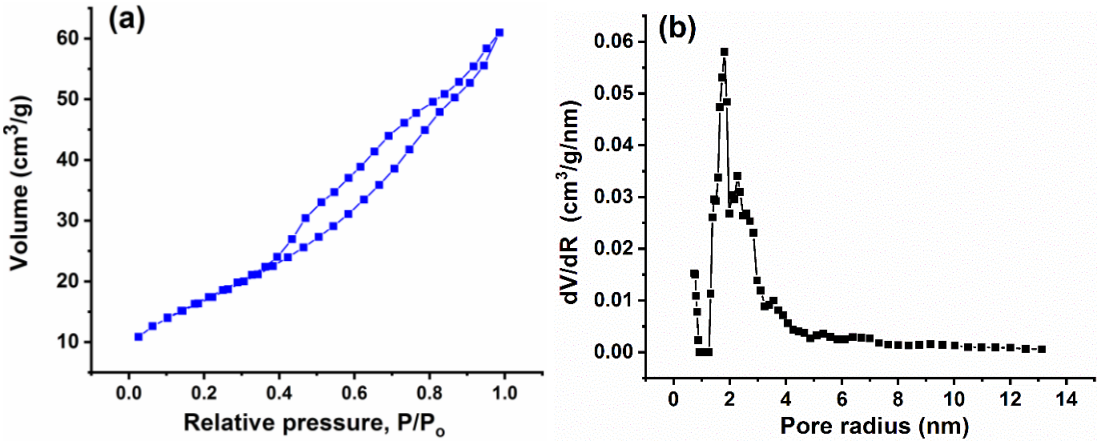

Fig. 3. (a) Adsorption/desorption isotherm of N_2 molecules by rutile TiO_2; **(b)** pore volume distribution by effective radius in rutile TiO_2.

Table 2

Morphological characteristics of rutile TiO_2 (average specific surface area and pore volume).

Sample	S_{BET} (m^2g^{-1})	S_{micro} (m^2g^{-1})	S_{meso}, (m^2g^{-1})		V_p, (cm^3g^{-1})	V_{micro} (cm^3g^{-1})	V_{meso} (cm^3g^{-1})
TiO_2-rutile	62	-	61.8		0.094	-	0.094

mesopores in associates is insignificant and is only 0.094 $cm \cdot g^{-1}$. The specific surface of flower-shaped associates is 62 $m^2 \cdot g^{-1}$.

2.5. IR spectral studies

The IR spectrum of each polymorphic modification of TiO_2 contains a certain set of spectral lines of the corresponding vibrational modes.

According to [22], the IR spectra of anatase are characterized by absorption bands of optical modes of symmetric vibrations A_{2u} of TiO_6 octahedra – 755 cm^{-1} (LO – longitudinal mode); 347 cm^{-1} (LO) and degenerate vibrations E_u – 350 cm^{-1} (LO); 438 cm^{-1} (TO – transverse mode); 365 cm^{-1} (LO); 272 cm^{-1} (TO), and rutile has absorption bands of symmetric vibrations A_{2u} – 796 cm^{-1} (LO); 172 cm^{-1} (TO) and degenerate vibrations E_u – 831 cm^{-1} (LO); 508 cm^{-1} (TO); 443 cm^{-1} (LO); 382 cm^{-1} (TO), 367 cm^{-1} (TO) and 189 cm^{-1} (TO). The authors of [23] give somewhat different frequency characteristics of the absorption bands for anatase – 850 cm^{-1}, 650 cm^{-1}, 480 cm^{-1}, 330 cm^{-1}, 265 cm^{-1}, 180 cm^{-1}, and for rutile – 620 cm^{-1}, 520 cm^{-1}, 420 cm^{-1}, 325 cm^{-1}, 190 cm^{-1}.

Fig. 4-a shows the IR spectrum of rutile TiO_2 synthesized by the liquid-phase acid method – boiling a solution of the titanium aquacomplex $[Ti(OH_2)_6]^{3+} \bullet 3Cl^-$. In this range, the absorption bands can be clearly identified by the maxima at 542 cm^{-1}, 409 cm^{-1} and 347 cm^{-1}. The band at 1630 cm^{-1}, insignificant in intensity, belongs to deformation vibrations of adsorbed water molecules [21].

At the initial stage of rutile synthesis, namely, in the first minutes of boiling the base precursor solution, $Ti(OH)_3Cl \bullet 2H_2O$ molecules are formed.

Their IR spectrum (Fig. 4-a) contains bands at 885 cm^{-1} and 359 cm^{-1} (A_{2u} mode) and 543 cm^{-1} and 413 cm^{-1} (E_u mode). The band at 1623 cm^{-1} corresponds to the deformation vibrations of H_2O in the titanium-containing hydrate molecules. Analyzing the frequency characteristics of the absorption bands in the spectra of rutile and $Ti(OH)_3Cl \bullet 2H_2O$ molecules, it can be found that the frequencies of the bands of degenerate vibrations E_u of crystalline TiO_2 and titanium-containing molecules are very close. This is primarily due to the equality of the geometric parameters of the rutile octahedra and titanium-containing hydrate molecules.

In the IR spectrum of anatase TiO_2 (Fig. 4-b), by the sol-gel method, namely, by combining a solution of the titanium aquacomplex $[Ti(OH_2)_6]^{3+} \bullet 3Cl^-$ with NaOH solution and heating the reaction mixture at a temperature of (40-60) ^0C [21], there are bands at 726 cm^{-1}, 339 cm^{-1} (A_{2u} mode) and 638 cm^{-1}, 550 cm^{-1}, 475 cm^{-1} (E_u mode).

When NaOH solution is dropwise introduced into $[Ti(OH_2)_6]^{3+} \bullet 3Cl^-$ precursor solution without heating the mixture, titanium-containing hydrate molecules $Ti(OH)_4 \bullet 2H_2O$ are formed already at pH ~ 2.0. The IR spectrum of these molecules (Fig. 4-b) shows bands at 880 cm^{-1}; 368 cm^{-1} (A_{2u} mode) and 640 cm^{-1}; 548 cm^{-1}; 472 cm^{-1} (E_u mode).

Comparing the frequency characteristics of the absorption bands in the spectra of anatase and $Ti(OH)_4 \bullet 2H_2O$ molecules, it can be seen that the frequencies of the bands of degenerate vibrations E_u are also very close, which indicates the equality of the geometric parameters of the anatase octahedra and molecules of hydrated titanium hydroxide.

The shift of the bands of the E_u optical mode of rutile in the direction of lower frequencies compared to the bands of this optical mode of anatase indicates that the average Ti-O interatomic distance in rutile octahedra is greater than this interatomic distance in anatase octahedra.

The larger average Ti-O interatomic distance in TiO_5Cl octahedra compared to this distance in TiO_6 octahedra is due to a decrease in the covalent component in bonds due to the weak polarizing effect of Cl^- anions on Ti^{4+} cations. The polarizing effect of an anion is estimated

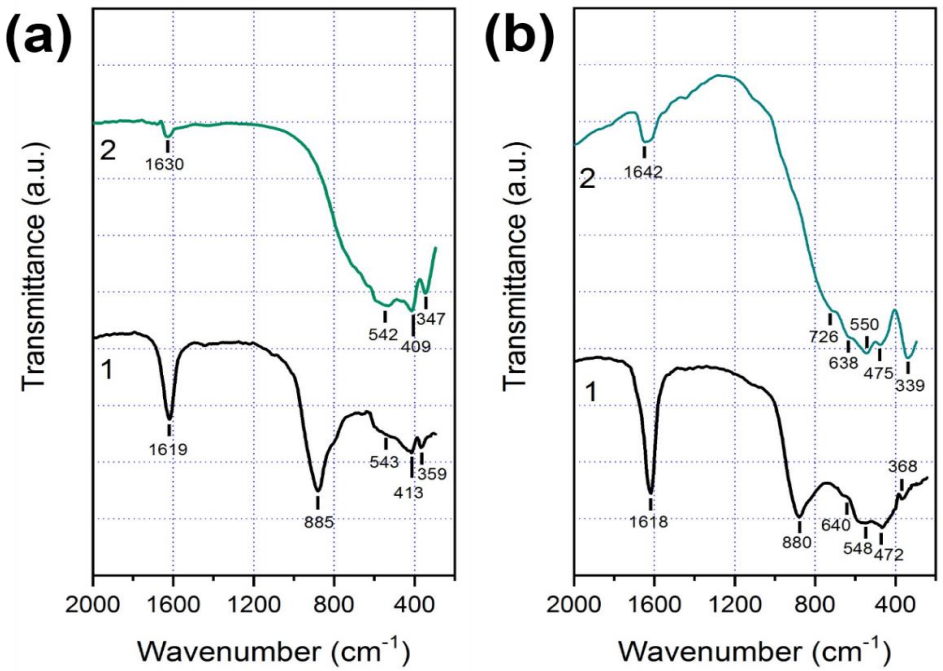

Fig. 4. (a) IR spectra of rutile TiO_2 (2) and $Ti(OH)_3Cl \bullet 2H_2O$ hydrate molecules involved in rutile structure formation of (1); **(b)** IR spectra of rutile TiO_2 (2) and $Ti(OH)_4 \bullet 2H_2O$ hydrate molecules involved in anatase structure formation (1).

from its ionic potential [24]. The value of the ionic potential is calculated by dividing the charge of the anion by its radius. The ionic potential of OH^- anion is 0.71 and exceeds the ionic potential of Cl^- anion – 0.49 [25,26].

2.6. Discussion of the results

The sol-gel synthesis of rutile using a titanium aquacomplex precursor provides the formation of very small rod-shaped particles (1–3) nm in diameter and (10–30) nm in length [21]. The specific surface of the product is 278 $m^2 \cdot g^{-1}$, and the pore volume is 0.61 $cm^2 \cdot g^{-1}$. This TiO_2 does not have photocatalytic properties. The reason for this is the small size of the particles and their high porosity.

Under other conditions, namely, when a titanium aquacomplex precursor solution is boiled, the explosive collapse of bubbles causes hydraulic shocks, which activate the condensation process in the reaction medium. This leads to the formation of much larger rod-shaped rutile particles with a diameter of (8-20) nm and a length of (30-80) nm. Their pore volume is not large and amounts to 0.094 $cm^2 \cdot g^{-1}$. According to [27–29], bubble collapse causes a local increase in temperature (~5000 K) and pressure (~1000 atm) in the reaction medium. The rate of local heating and cooling of the medium is > 10^9 $K \cdot s^{-1}$. The structural and morphological characteristics of the synthesized TiO_2 provide it with a high photocatalytic activity.

Thus, the thermolytic decomposition of the aquacomplex precursor $[Ti(OH_2)_6]^{3+} \bullet 3Cl^-$ in a chloride-acid medium, due to its boiling, is accompanied by the formation of $Ti(OH)_3 \bullet 2H_2O$ hydrate molecules, which form a rutile structure upon condensation. This scheme of phase formation can also be implemented in the pyrogenic synthesis of TiO_2 [14]. During the combustion of $TiCl_4$ in a hydrogen-air flame during the rapid course of reactions involving H_2O molecules and Cl atoms, it is possible to form not only hydrate molecules $Ti(OH)_4 \bullet 2H_2O$, which provide the formation of anatase upon condensation, but also hydrate molecules $Ti(OH)_3Cl \bullet 2H_2O$, which lead to the formation of the rutile phase.

2.7. Kinetic studies

The efficiency of the synthesized rutile TiO_2 photocatalyst was evaluated under UV irradiation using LEDs with a wavelength of 365 nm. The effect of independent parameters on the efficiency of CR photodegradation was studied: the concentration of the photocatalyst and H_2O_2 in the previously specified ranges (Table 1). Before the start of irradiation, adsorption-desorption was performed for 20 min for all experiments. It has been established that the removal of CR upon adsorption in the dark is insignificant compared to CR photodegradation in the presence of UV irradiation. Fig. 5-a shows the effect of TiO_2 photocatalyst loading in the range of 0.5–1.5 g/L on degradation of CR (5 mg/L). It is clearly seen in Fig. 5 that the efficiency of CR photodegradation increases with an increase in the photocatalyst loading, however, a further increase to 1.5 g/L leads to blocking of the penetration of UV light into the volume of the reaction mixture, and the efficiency of CR degradation decreases. In addition, a decrease in the rate of CR degradation at a higher catalyst loading is a consequence of the deactivation of activated molecules upon collision with ground state molecules. The authors of [30] also reported on excessive agglomeration and sedimentation of TiO_2 particles at high photocatalyst loading. The synthesized TiO_2 sample is difficult to remove from the medium because it is well dispersed in an aqueous solution. This is advantageous as it allows the same powder left over from the first photodegradation cycle to be reused and several more cycles of CR photodegradation to be carried out.

The efficiency of synthesized TiO_2 and Degussa P25 were compared under identical experimental conditions (Fig. 6). Sample Degussa P25 was found to adsorb CR molecules resulting in a decrease in degradation rate. Since the amount of dye adsorbed on the surface of the catalyst increases, active centers are blocked, which leads to a decrease in the rate of formation of •OH radicals.

The effect of the concentration of H_2O_2 on the activity of the rutile photocatalyst during CR degradation was studied in the range from 0 to 5 mM; the results are shown in Fig. 8 (a, b, c). It has been found that the efficiency of CR degradation increases with an increase in the concentration of H_2O_2, which is associated with the formation of a large amount of hydroxyl radicals under the action of TiO_2 and UV radiation.

For a concentration of 0.5 g/L TiO_2, an increase in the reaction rate constant from 0.2070 to 1.5544 min^{-1} is observed with an increase in the concentration of H_2O_2 from 0 to 5 mM. For a concentration of 1.0 g/L TiO_2, an

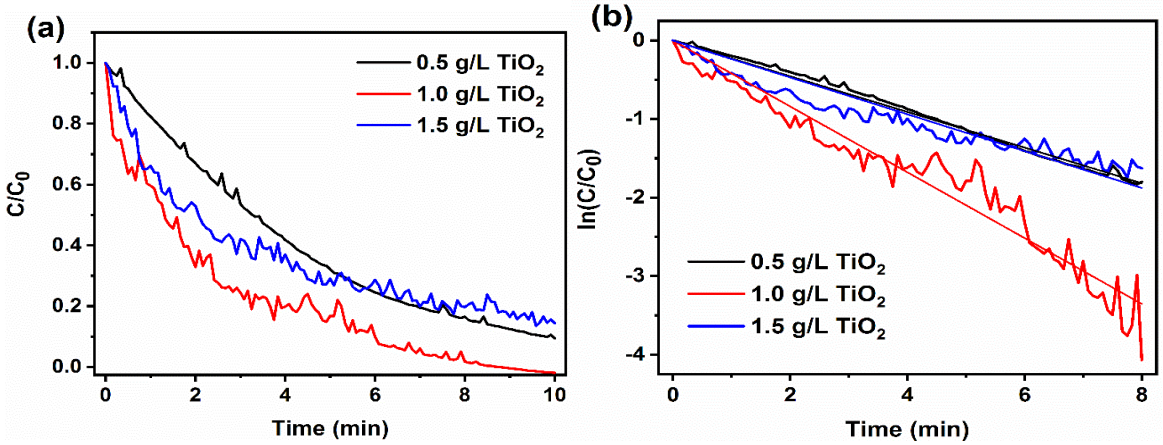

Fig. 5. (a) Real-time monitoring of photocatalytic degradation of CR dye using 0.5 g/L, 1.0 g/L and 1.5 g/L TiO_2; **(b)** kinetic lines transformed according to the first-order kinetic model.

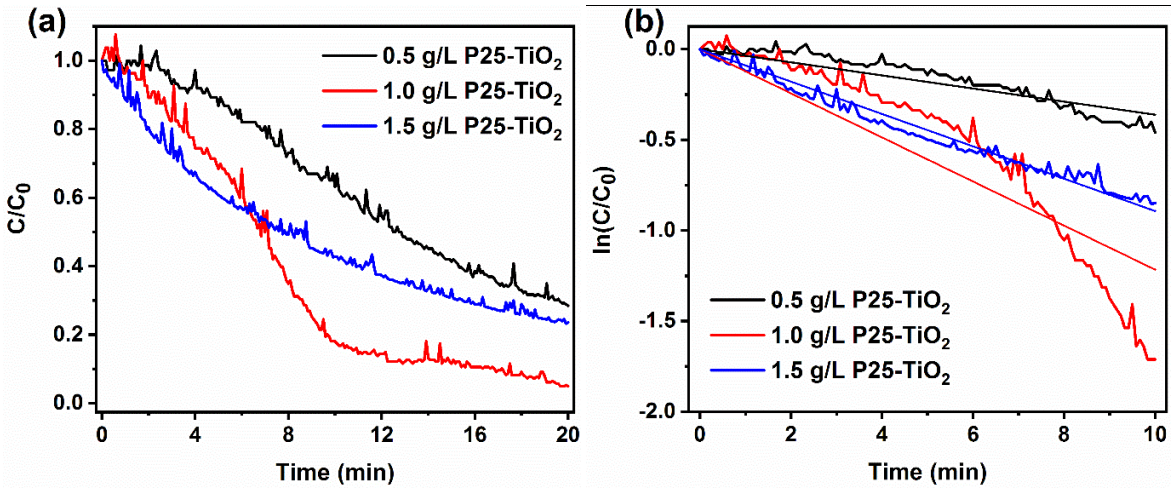

Fig. 6. (a) Real-time monitoring of photocatalytic degradation of CR dye using 0.5 g/L, 1.0 g/L and 1.5 g/L P25-TiO_2; **(b)** kinetic lines transformed according to the first-order kinetic model.

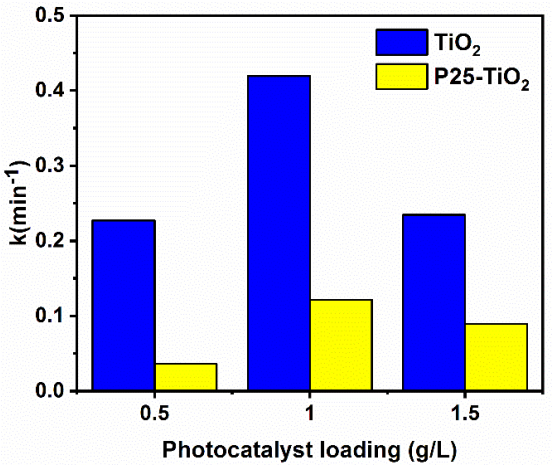

Fig. 7. Comparison of the efficiency of TiO_2 and P25-TiO_2 samples in CR photodegradation.

increase in the reaction rate constant from 0.4987 to 1.8414 min^{-1} is observed with an increase in the concentration of H_2O_2 from 0 to 5 mM. For a concentration of 1.5 g/L TiO_2, a rapid increase in the reaction rate constant from 0.3023 to 2.1959 min^{-1} is observed with an increase in the concentration of H_2O_2 from 0 to 5 mM. Obtained logarithmic curves (Fig. 8 (d, e, f)) are characterized by high correlation coefficients (R^2) from 0.9247 to 0.9973 (Table 3).

Cyclic CR photodegradation experiments were performed to confirm the stability of synthesized rutile TiO_2 (Fig. 9-a). The duration of repeated photodegradation experiments was 10 min. The results obtained show that the TiO_2 sample retains photocatalytic activity for seven consecutive cycles of use. However, the reaction rate constant decreases slightly (Fig. 9-b). During photodegradation of Congo Red, k values decrease from 1.8414 to 1.1330 min^{-1} (Fig. 9-b). The synthesized sample was found to exhibit higher photocatalytic activity and greater stability than Degussa P25 even after the seventh cycle of CR photodegradation.

For comparison, cyclic CR degradation experiments were performed using a commercial P25-TiO_2 photocatalyst (Fig. 10-a). The duration of repeated CR photodegradation experiments was 10 min. The results obtained show that the activity of the P25-TiO_2 sample rapidly decreases as a result of seven consecutive cycles of use. The reaction rate constant noticeably decreases from 1.0722 to 0.5533 min^{-1} (Fig. 10-b).

2.8. Response Surface Methodology

2.8.1. Model Equation

To analyze the dual effect of two variable parameters, synthesized photocatalyst concentration (A) and H_2O_2 concentration (B), on the photodegradation efficiency of Congo Red, equation (9) was derived in the RSM experimental project. Table 4 lists the experiments performed and the experimental and expected values of CR photodegradation under UV irradiation in a batch photoreactor.

Experimental data were processed by four different models: linear, two-factor interaction (2FI), quadratic and cubic models to obtain regression equations. Various tests, sum of squares and model summary statistics, were conducted to determine the reliability of the models, the results are presented in Tables 5-6. The results obtained are used to select the best model based on the p-value criterion (Table 5). The main criteria for comparing models and confirming the adequacy of the selected model are calculated statistical data. The statistics include the following criteria: Adjusted R^2, R^2, and Predicted Residual Error Sum of Squares (PRESS). A good model

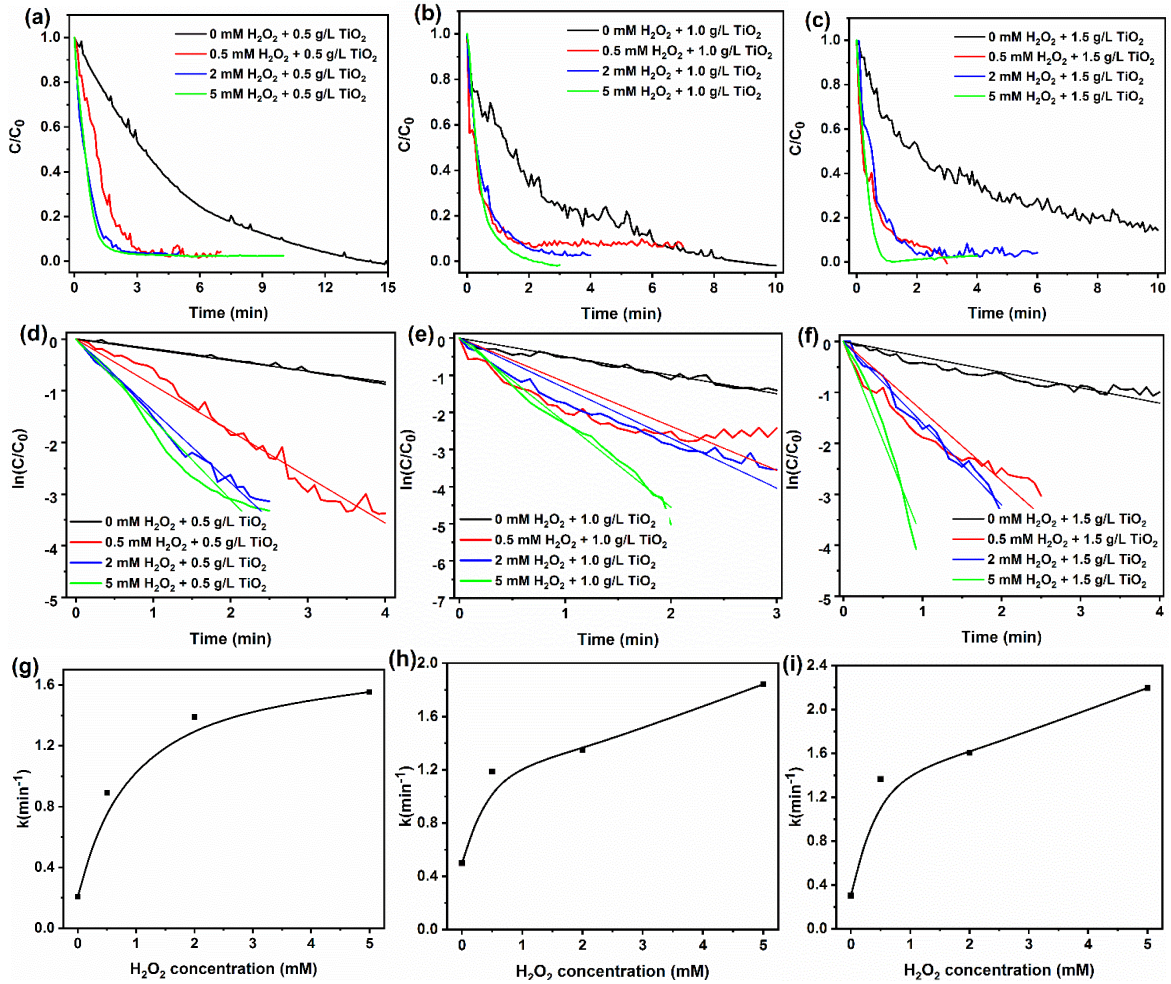

Fig. 8. Real-time monitoring of photocatalytic degradation of CR dye using (a) 0.5 g/L, (b) 1.0 g/L, (c) 1.5 g/L TiO_2; (d, e, f) kinetic lines transformed according to the first-order kinetic model; (g, h, i) reaction rate constants as functions of the concentration of H_2O_2. The initial concentration of CR is 5 mg/L.

Table 3

Rate constants of the first order kinetic model of CR photodegradation with a TiO_2 sample (experimental conditions: solution volume 25 mL, dye concentration 5 mg/L, T = 293 K).

Photocatalyst loading (g/L)	Concentration of H_2O_2 (mM)							
	0		0.5		2.0		5.0	
	k, min^{-1}	R^2	k, min^{-1}	R^2	k, min^{-1}	R^2	k, min^{-1}	R^2
0.5 g/L	0.2070	0.9973	0.8902	0.9929	1.3895	0.9949	1.5544	0.9887
1.0 g/L	0.4987	0.9892	1.1855	0.9247	1.3458	0.9833	1.8414	0.9967
1.5 g/L	0.3023	0.9738	1.3651	0.9654	1.6036	0.9961	2.1959	0.9831

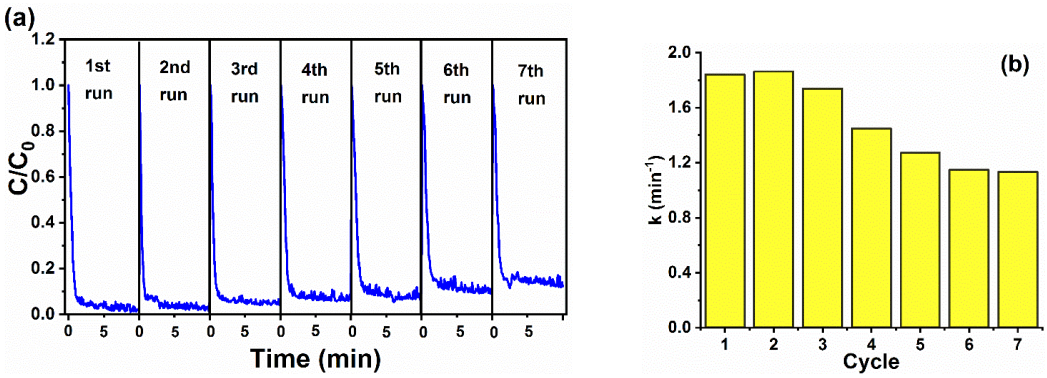

Fig. 9. (a) Cyclic activity testing of the synthesized TiO_2 photocatalyst using CR; **(b)** Rate constants of repeated degradation reactions of the CR dye (5 mg/L). The initial concentration of hydrogen peroxide was 5 mM and the initial concentration of TiO_2 was 1 g/L.

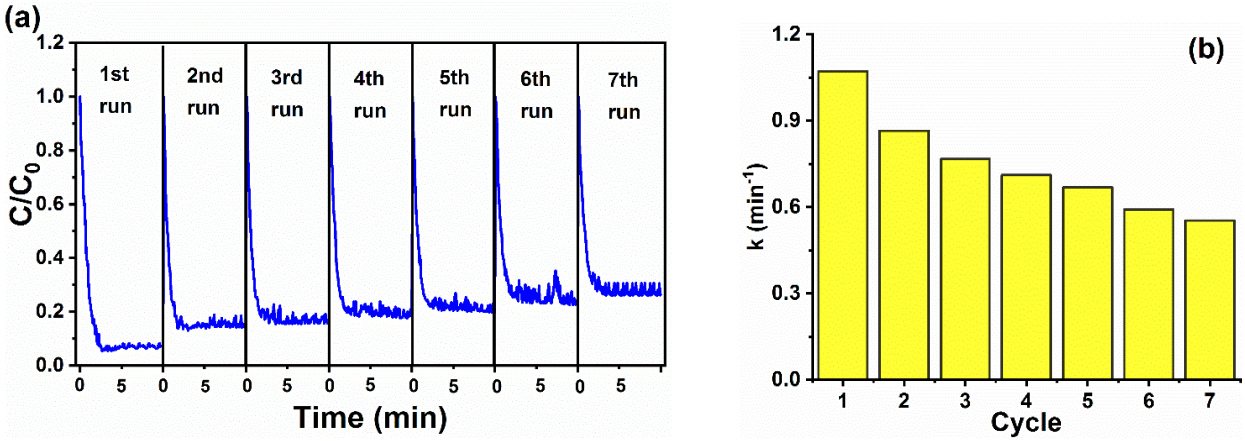

Fig. 10. (a) Cyclic activity testing of a commercial P25-TiO_2 photocatalyst using CR; **(b)** Rate constants of repeated degradation reactions of the CR dye (5 mg/L). The initial concentration of hydrogen peroxide was 5 mM, and the initial concentration of P25-TiO_2 was 1 g/L.

Table 4

Design with experimental and predicted values of reaction rate constant using equation (9).

Run	Experimental Conditions		Rate constant, min^{-1}	
	Photocatalyst loading (g/L)	Concentration of H_2O_2 (mM)	Experimental	Predicted
1	0.5	0	0.2070	0.421
2	0.5	0.5	0.8902	0.719
3	0.5	2	1.3895	1.364
4	0.5	5	1.5544	1.538
5	1.0	0	0.4987	0.554
6	1.0	0.5	1.1855	0.872
7	1.0	2	1.3458	1.576
8	1.0	5	1.8414	1.869
9	1.5	0	0.3023	0.629
10	1.5	0.5	1.3651	0.966
11	1.5	2	1.6036	1.730
12	1.5	5	2.1959	2.141

should have a high predicted R^2 and a low PRESS.

According to the above criteria, the quadratic model has rather high values of adjusted R^2 (0.7723), R^2 (0.8758) and is characterized by the lowest PRESS value (1.67). Thus, a quadratic model was finally chosen for constructing the surface and performing calculations.

The quadratic model obtained to describe the photocatalytic removal of CR from an aqueous solution using synthesized rutile TiO_2 is as follows:

$$\text{Rate constant } (min^{-1}) = 1.73 + 0.20 * C(TiO_2) + 0.66 * C(H_2O_2) + 0.099 * C(TiO_2) * C(H_2O_2) - 0.029 * C(TiO_2)^2 - 0.52 * C(H_2O_2)^2 \quad (9)$$

The ANOVA results of the quadratic model (equation (9)) for CR degradation are shown in Table 8. In the statistics presented, the validity of the model was confirmed by a large F value (8.46) and a small p value (< 0.0109). The accuracy of the model is also confirmed by the low coefficient of variation (CV) of 4.48%.

The coefficient of determination R^2 confirmed the reliability of the model; the value of the predicted R^2 = 0.7723 is consistent with the adjusted R^2 = 0.8758, which indicates that the resulting model is reliable. Fig. 11 shows the ratio of the experimental values of the rate constant of CR photodegradation reaction compared to the predicted values obtained from the RSM model.

2.8.2. Interaction Effects of Independent Operating Parameters

Using a quadratic model (Equation (9)) a three-dimensional (3D) model and a contour plot were created to represent the influence of independent parameters on the photodegradation efficiency of CR under the action of synthesized rutile TiO_2 and UV irradiation. On 3D and contour diagrams, one indicator is determined depending on the change in two independent parameters in the studied range, shown in Table 1. Fig. 12 shows the effect of the loading of the synthesized photocatalyst and H_2O_2 concentration on the efficiency of CR photodegradation under UV irradiation (at a constant CR concentration (5 mg/L)). The contour lines indicate an increase in the

Table 5

Adequacy of the tested model: sequential model sum of squares.

Source	Sum of squares	Degree of freedom	Mean square	F-value	P-value	Remarks
Linear	3.10	2	1.55	13.28	0.0021	
2FI	0.047	1	0.047	0.38	0.5561	
Quadratic	0.49	2	0.24	2.84	0.1357	Suggested
Cubic	0.44	3	0.15	5.67	0.0940	Aliased

Table 6

Adequacy of the tested model: model summary statistics.

Source	Standard Deviation	R^2	Adjusted R^2	Predicted R^2	PRESS	Remarks
Linear	0.34	0.7469	0.6907	0.5350	1.93	
2FI	0.35	0.7583	0.6677	0.3958	2.51	
Quadratic	0.29	0.8758	0.7723	0.5970	1.67	Suggested
Cubic	0.16	0.9814	0.9317	-0.2039	5.00	Aliased

Table 7

Coefficients of the quadratic equation.

Factor	Coefficient Estimate	Degree of Freedom	Standard Error	95% Confidence Interval Low	95% Confidence Interval High
Intercept	1.73	1	0.21	1.21	2.24
A	0.20	1	0.11	-0.064	0.47
B	0.66	1	0.11	0.39	0.93
AB	0.099	1	0.13	-0.23	0.42
A^2	-0.029	1	0.18	-0.47	0.41
B^2	-0.52	1	0.22	-1.05	0.015

Table 8

Analysis of variance (ANOVA) of the quadratic model (Equation (9)).

Source	Sum of Squares	Df	Mean Square	F - Value	P-value (Prob > F)
Model	3.64	5	0.73	8.46	0.0109
A	0.30	1	0.30	3.47	0.1117
B	3.10	1	3.10	36.04	0.0010
AB	0.047	1	0.047	0.55	0.4860
A^2	$2.297 \cdot 10^{-3}$	1	$2.297 \cdot 10^{-3}$	0.027	0.8760
B^2	0.49	1	0.49	5.65	0.0550
Residual	0.52	6	0.086		
Cor. Total	4.16	11			
	Adjusted R^2 = 0.8758	Predicted R^2 = 0.7723	Model precision = 8.293		
	Std. Dev. = 0.29	Mean = 1.20	CV = 4.48%		

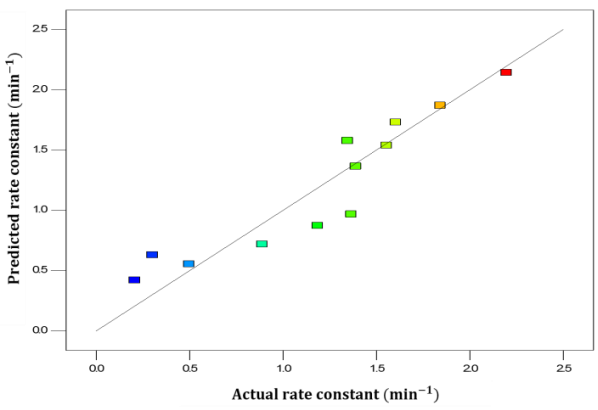

Fig. 11. Predicted degradation rate constants compared to actual experimental values.

efficiency of CR degradation with an increase in the loading of the rutile photocatalyst and the concentration of H_2O_2.

The results obtained show that the photocatalyst loading and the concentration of H_2O_2 have a significant effect on the degradation of CR. With the addition of H_2O_2, an improvement in the activity of the photocatalyst at the beginning of photooxidation is observed, which is associated with the formation of a large amount of hydroxyl radicals under the action of UV radiation. As shown in Fig. 12, in the absence of hydrogen peroxide and at a low concentration of the photocatalyst, 100% decomposition of the dye is not achieved within a reaction time of 10 min. The maximum efficiency of CR degradation is achieved at a constant initial CR concentration of 5 mg/L, for 10 min UV irradiation, at

H_2O_2 concentration of 5 mM, and a photocatalyst loading of 1.5 g/L (Fig. 12). However, a further increase in the concentration of H_2O_2 leads to the recombination of the formed hydroxyl radicals by excess H_2O_2 molecules, and the efficiency of CR decomposition decreases. There is a positive charge on the surface of the photocatalyst, which attracts OH^- ions formed in the solution due to the dissociation of H_2O_2, which significantly increases the rate of the CR photodegradation. It is known that the electron-hole pair formed on the catalyst surface improves the photodegradation rate of dyes [31]. An increase in the photocatalyst loading from 0.5 to 1.5 g/L blocks the penetration of UV radiation into the volume of the reaction mixture, and the efficiency of CR degradation first increases and then decreases.

2.8.3. Numerical Optimization

The main goal of the study was to find the optimal parameters for the process of photodegradation of CR in an aqueous solution. The presented model, which is able to predict the maximum activity of the photocatalyst, has shown that the optimal values of the process variables are H_2O_2 concentration of 5 mM and the photocatalyst concentration of 1.5 g/L. Under these conditions, the predicted reaction rate constant of CR under UV irradiation is 2.1959 min^{-1}, which is in good agreement with the experimental value of 2.1410 min^{-1}. A comparison of the photocatalytic activity of various TiO_2-based materials with respect to the photodegradation of Congo Red is presented in Table 9.

Conclusions

In this work, the photodegradation of Congo Red in an aqueous solution using rutile TiO_2 synthesized by thermolytic decomposition of a titanium aquacomplex precursor solution $[Ti(OH_2)_6]^{3+}•3Cl^-$ has been studied.

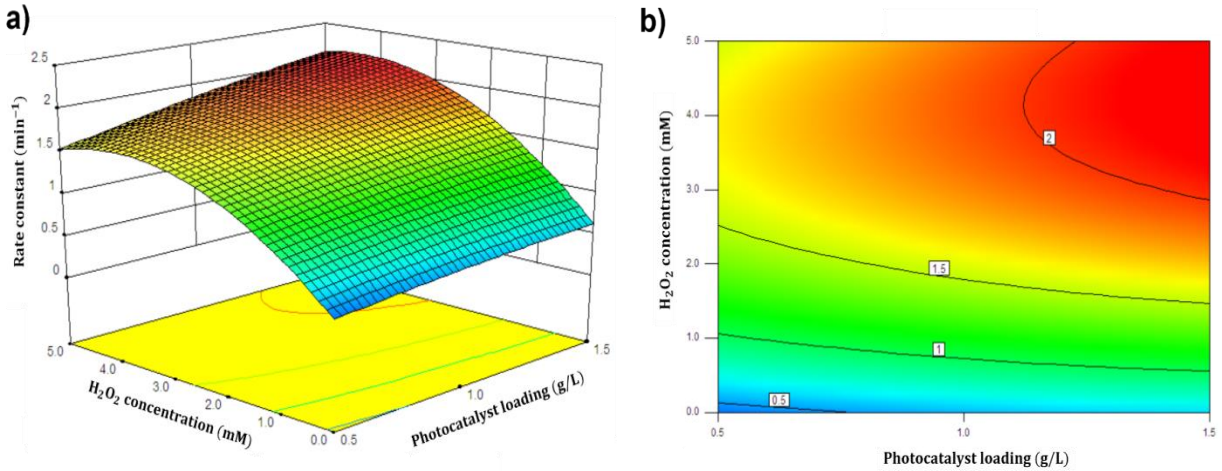

Fig. 12. Effect of photocatalyst loading and H_2O_2 concentration on CR photodegradation rate constant: CR concentration was kept constant (5 mg/L).

Table 9

Comparison of the photodegradation extent of Congo Red in the presence of various catalysts.

Type of catalyst	Condition	Degradation extent, %	Refs
Nano-TiO_2	CR (20 mg/L) under UV irradiation (20 min)	94	[30]
TiO_2	CR (10 mg/L) under UV irradiation (180 min)	97.3	[3]
RM-TiO_2	CR (5 mg/L), H_2O_2 (15 mM) under UV irradiation (50 min)	92.7	[1]
LT-TiO_2	CR (5 mg/L), H_2O_2 (10 mM) under UV irradiation (30 min)	99.9	[1]
TiO_2/SA	CR (40 mg/L), H_2O_2 (20 mM) under visible light irradiation (210 min)	100	[32]
Ni–TiO_2	CR (10 mg/L) under UV irradiation (180 min)	92.31	[2]
2% Fe^{3+}-doped TiO_2	CR (5 mg/L), H_2O_2 (20 mM) under UV irradiation (30 min)	99.4	[33]
Mg-TiO_2-P25/PMS	CR ($2.5*10^{-5}$ M) under visible light irradiation (120 min)	95	[34]
TiO_2 doped cobalt ferrite	CR (10 mg/L) under visible light irradiation (120 min)	97	[35]
TiO_2	CR (5 mg/L), H_2O_2 (5 mM) under UV irradiation (10 min)	100	This work

The effect of the concentration of TiO_2, UV irradiation, and the concentration of H_2O_2 on CR photodegradation has been studied in detail. It has been found that rutile TiO_2 can readily decompose 5 mg/L CR dye within 10 min of UV irradiation. The CR photodegradation reaction is well described by the first-order reaction kinetics. The TiO_2 concentration of 1.5 g/L and the H_2O_2 concentration of 5 mM proved to be the most effective, leading to complete decomposition of CR in 10 min at a reaction rate constant of 2.1959 min^{-1}. Under identical conditions, the photocatalytic activity of the synthesized rutile TiO_2 is 3.5 times higher than the activity of P25 titanium dioxide produced by the German concern Evonik. In addition, the synthesized TiO_2 sample can be reused for seven cycles of CR photodegradation. In particular, the resulting TiO_2 exhibits higher photocatalytic activity than Degussa P25 even after the seventh cycle of CR photodegradation. The increase in the photocatalytic efficiency of TiO_2 with the addition of H_2O_2 is explained by the formation of a large amount of hydroxyl radicals, which cause the rapid destruction of CR molecules. The synthesized rutile photocatalyst can be used to treat wastewater from organic toxicants.

Acknowledgment

The authors thank the Ministry of Education and Science of Ukraine for financial support in the framework of project 0120U102035.

Mironyuk Ivan – Doctor of Chemical Sciences, Head of the Department of Chemistry, Vasyl Stefanyk Precarpathian National University;
Danyliuk Nazarii – PhD student, leading specialist at the Educational and Scientific Center of Material Science and Nanotechnology, Vasyl Stefanyk Precarpathian National University;
Turovska Liliia – Associate Professor of the Department of Medical Informatics, Medical and Biological Physics, Ivano-Frankivsk National Medical University;
Mykytyn Ihor – Associate Professor of the Chemistry Department, Vasyl Stefanyk Precarpathian National University.

[1] T. Tatarchuk, N. Danyliuk, A. Shyichuk, W. Macyk, M. Naushad, *Photocatalytic degradation of dyes using rutile TiO_2 synthesized by reverse micelle and low temperature methods: real-time monitoring of the degradation kinetics*, J. Mol. Liq., 342, 117407 (2021); https://doi.org/10.1016/j.molliq.2021.117407.
[2] K. Indira, S. Shanmugam, A. Hari, S. Vasantharaj, S. Sathiyavimal, K. Brindhadevi, A. El Askary, A. Elfasakhany, A. Pugazhendhi, *Photocatalytic degradation of congo red dye using nickel–titanium dioxide nanoflakes synthesized by Mukia madrasapatna leaf extract*, Environ. Res., 202, 111647 (2021); https://doi.org/10.1016/j.envres.2021.111647.
[3] J. Wang, Y. Jiang, Z. Zhang, G. Zhao, G. Zhang, T. Ma, W. Sun, *Investigation on the sonocatalytic degradation of congo red catalyzed by nanometer rutile TiO_2 powder and various influencing factors*, Desalination, 216, 196 (2007); https://doi.org/10.1016/j.desal.2006.11.024.
[4] T. Tatarchuk, A. Shyichuk, Z. Sojka, J. Gryboś, M. Naushad, V. Kotsyubynsky, M. Kowalska, S. Kwiatkowska-Marks, N. Danyliuk, *Green synthesis, structure, cations distribution and bonding characteristics of superparamagnetic cobalt-zinc ferrites nanoparticles for Pb(II) adsorption and magnetic hyperthermia applications*, J. Mol. Liq., 328, 115375 (2021); https://doi.org/10.1016/j.molliq.2021.115375.
[5] I. Mironyuk, I. Mykytyn, H. Vasylyeva, K. Savka, *Sodium-modified mesoporous TiO_2: Sol-gel synthesis, characterization and adsorption activity toward heavy metal cations*, J. Mol. Liq., 316, 113840 (2020); https://doi.org/10.1016/j.molliq.2020.113840.
[6] S. Foteinis, E. Chatzisymeon, *Heterogeneous photocatalysis for water purification*, INC, 2020. https://doi.org/10.1016/B978-0-12-817836-2.00004-1.
[7] Z. Wei, J. Liu, W. Shangguan, *A review on photocatalysis in antibiotic wastewater: Pollutant degradation and hydrogen production*, Chinese J. Catal., 4, 1440 (2020); https://doi.org/10.1016/S1872-2067(19)63448-0.
[8] M.E. Borges, M. Sierra, E. Cuevas, R.D. García, P. Esparza, *Photocatalysis with solar energy: Sunlight-responsive photocatalyst based on TiO_2 loaded on a natural material for wastewater treatment*, Sol. Energy, 135 (2016) 527–535. https://doi.org/10.1016/j.solener.2016.06.022.
[9] M. Curti, D.W. Bahnemann, C.B. Mendive, Mechanisms in Heterogeneous Photocatalysis: Titania under UV and Visible Light Illumination, Elsevier Ltd., 2016; https://doi.org/10.1016/b978-0-12-803581-8.03800-5.
[10] H. Chakhtouna, H. Benzeid, N. Zari, A. el kacem Qaiss, R. Bouhfid, *Recent progress on Ag/TiO_2 photocatalysts: photocatalytic and bactericidal behaviors*, Environ. Sci. Pollut. Res., 28 44638 (2021); https://doi.org/10.1007/s11356-021-14996-y.
[11] G. Sujatha, S. Shanthakumar, F. Chiampo, *UV light-irradiated photocatalytic degradation of coffee processing wastewater using TiO_2 as a catalyst*, Environ, 7, 1 (2020); https://doi.org/10.3390/environments7060047.
[12] P. Billik, G. Plesch, V. Brezová, L. Kuchta, M. Valko, M. Mazúr, *Anatase TiO_2 nanocrystals prepared by mechanochemical synthesis and their photochemical activity studied by EPR spectroscopy*, J. Phys. Chem. Solids, 68, 1112 (2007), https://doi.org/10.1016/j.jpcs.2007.02.010.
[13] A. Dodd, A. McKinley, T. Tsuzuki, M. Saunders, *Optical and photocatalytic properties of nanocrystalline TiO_2 synthesised by solid-state chemical reaction*, J. Phys. Chem. Solids, 68, 2341 (2007); https://doi.org/10.1016/j.jpcs.2007.07.008.
[14] H.D. Jang, S.K. Kim, S.J. Kim, *Effect of particle size and phase composition of titanium dioxide nanoparticles on the photocatalytic properties*, J. Nanoparticle Res., 3 (2001) 141–147. https://doi.org/10.1023/A:1017948330363.

[15] H. Park, H.S. Jie, B. Neppolian, K. Tsujimaru, J.P. Ahn, D.Y. Lee, J.K. Park, M. Anpo, *Preparation of highly active TiO_2 nano-particle photocatalysts by a flame aerosol method for the complete oxidation of 2-propanol*, Top. Catal., 47, 166 (2008); https://doi.org/10.1007/s11244-007-9019-2.
[16] G.L. Chiarello, E. Selli, L. Forni, *Photocatalytic hydrogen production over flame spray pyrolysis-synthesised TiO_2 and Au/TiO_2*, Appl. Catal. B Environ., 84, 332 (2008); https://doi.org/10.1016/j.apcatb.2008.04.012.
[17] V.M. Gun'ko, V.V. Turov, *Nuclear magnetic resonance studies of interfacial phenomena*, CRC Press. Boca Rat. (2013). https://doi.org/10.1201/b14202.
[18] A. Singh, S. Kumar, *Structural, chemical, optical and photocatalytic properties of Zr co-doped anatase-rutile mixed phase TiO_2: Ag nanoparticles*, J. Alloys Compd., 925, 166709 (2022); https://doi.org/10.1016/j.jallcom.2022.166709.
[19] M.Z. Bin Mukhlish, F. Najnin, M.M. Rahman, M.J. Uddin, *Photocatalytic Degradation of Different Dyes Using TiO_2 with High Surface Area: A Kinetic Study*, J. Sci. Res., 5 301–314 (2013); https://doi.org/10.3329/jsr.v5i2.11641.
[20] A. Golub, A. Tyshchenko, I. Kokot, *Investigation of the solubility of Ti(OH)4 in chlorine and hydrochloric acids*, Journal of Applied Chemistry, XLIII, 2129–2134 (1970).
[21] L.I. Myronyuk, I.F. Myronyuk, V.L. Chelyadyn, V.M. Sachko, M.A. Nazarkovsky, R. Leboda, J. Skubiszewska-Zięba, V.M. Gun'ko, *Structural and morphological features of crystalline nanotitania synthesized in different aqueous media*, Chem. Phys. Lett., 583 (2013) 103–108. https://doi.org/10.1016/j.cplett.2013.07.068.
[22] G. Busca, G. Ramis, J.M.G. Amores, V.S. Escribano, P. Piaggio, *FT Raman and FTIR studies of titanias and metatitanate powders*, J. Chem. Soc. Faraday Trans., 90 (1994) 3181–3190. https://doi.org/10.1039/FT9949003181.
[23] R.J. Gonzalez, Raman, X-ray, and EELS Studies of Nanophase Titania, Thesis. (1996).
[24] V.A. Frink-Kamenetsky, Essays on crystal chemistry, Chemistry. (1974) 496.
[25] M. Bairamov, Fundamental electrochemistry, Academia. (2005).
[26] A.R. West, Solid state chemistry and its applications, 1991. https://doi.org/10.1107/s0108768185002476.
[27] M.D. Bleši, Z. V. Šaponji, J.M. Nedeljkovi, D.P. Uskokovi, *TiO_2 films prepared by ultrasonic spray pyrolysis of nanosize precursor*, Mater. Lett., 54, 298 (2002); https://doi.org/10.1016/S0167-577X(01)00581-X.
[28] W.L. Guo, X.K. Wang, Z.M. Lin, G.Z. Song, *Sonochemical Synthesis of Nanocrystalline TiO_2 by Hydrolysis of Titanium Alkoxides*, Microelectron. Eng., 66, 95 (2003); https://doi.org/10.1016/S0167-9317(03)00031-5.
[29] W. Huang, X. Tang, Y. Wang, Y. Koltypin, A. Gedanken, *Selective synthesis of anatase and rutile via ultrasound irradiation*, Chem. Commun., 1415 (2000); https://doi.org/10.1039/b003349i.
[30] S. Erdemoğlu, S.K. Aksu, F. Sayilkan, B. Izgi, M. Asiltürk, H. Sayilkan, F. Frimmel, Ş. Güçer, *Photocatalytic degradation of Congo Red by hydrothermally synthesized nanocrystalline TiO_2 and identification of degradation products by LC-MS*, J. Hazard. Mater., 155, 469 (2008); https://doi.org/10.1016/j.jhazmat.2007.11.087.
[31] N. Danyliuk, T. Tatarchuk, K. Kannan, A. Shyichuk, *Optimization of TiO_2-P25 photocatalyst dose and H_2O_2 concentration for advanced photooxidation using smartphone-based colorimetry*, Water Sci. Technol., 84, 469 (2021); https://doi.org/10.2166/wst.2021.236.
[32] H.X. Guo, K.L. Lin, Z.S. Zheng, F. Bin Xiao, S.X. Li, *Sulfanilic acid-modified P25-TiO_2 nanoparticles with improved photocatalytic degradation on Congo red under visible light*, Dye. Pigment, 92, 1278 (2012); https://doi.org/10.1016/j.dyepig.2011.09.004.
[33] I. Mironyuk, N. Danyliuk, T. Tatarchuk, I. Mykytyn, V. Kotsyubynsky, *Photocatalytic degradation of Congo red dye using Fe-doped TiO_2 nanocatalysts*, Phys. Chem. Solid State, 22, 697 (2021); https://doi.org/10.15330/pcss.22.4.697-710.
[34] U.O. Bhagwat, J.J. Wu, A.M. Asiri, S. Anandan, *Sonochemical Synthesis of Mg-TiO_2 nanoparticles for persistent Congo red dye degradation*, J. Photochem. Photobiol. A Chem., 346, 559 (2017); https://doi.org/10.1016/j.jphotochem.2017.06.043.
[35] C.M. Magdalane, G.M.A. Priyadharsini, K. Kaviyarasu, A.I. Jothi, G.G. Simiyon, *Synthesis and characterization of TiO_2 doped cobalt ferrite nanoparticles via microwave method: Investigation of photocatalytic performance of congo red degradation dye*, Surfaces and Interfaces, 25, 101296 (2021); https://doi.org/10.1016/j.surfin.2021.101296.

Іван Миронюк[1], Назарій Данилюк[1], Лілія Туровська[2], Ігор Микитин[1]

Структурно-морфологічні та фотокаталітичні властивості TiO_2, отриманого термолітичним розкладом аквакомплексу $[Ti(OH_2)_6]^{3+}•3Cl^-$

[1]Хімічний факультет Прикарпатського національного університету імені Василя Стефаника, Івано-Франківськ, Україна, myrif555@gmail.com
[2]Навчально-науковий центр матеріалознавства і нанотехнологій Прикарпатського національного університету імені Василя Стефаника, Івано-Франківськ, Україна, danyliuk.nazariy@gmail.com
[3]Кафедра медичної інформатики, медичної та біологічної фізики Івано-Франківського національного медичного університету, Івано-Франківськ, Україна, lturovska@ifnmu.edu.ua

Термолітичний розклад у хлориднокислотному середовищі розчину титанового аквакомплексного прекурсору $[Ti(OH_2)_6]^{3+}•3Cl$, в результаті його кип'ятіння за температури (110-114) ^0C, супроводжується гідролізом прекурсору та утворенням молекул-гідратів $Ti(OH)_3Cl • 2H_2O$, які внаслідок конденсації забезпечують одержання рутильного TiO_2 з стержневидною формою частинок довжиною (30-80) нм і діаметром (8-20) нм, об'єднаних у свою чергу в квітковидні асоціати діаметром (200-280) нм. Питома поверхня асоціатів 62 $м^2 \cdot г^{-1}$. ІЧ-спектроскопічні дослідження продуктів гідролізу прекурсору та синтезованого оксидного матеріалу засвідчують, що геометричні параметри октаедрів TiO_5Cl молекул-гідратів $Ti(OH)_3Cl •2H_2O$ є близькими до параметрів октаедрів TiO_6 рутильного TiO_2. Середня міжатомна відстань Ti-O октаедрів титановмісних молекул-гідратів є своєрідним шаблоном, який скеровує процес кристалізації TiO_2 на утворення рутилу. Синтезований в такий спосіб рутильний нанопорошковий TiO_2 являється ефективним фотокаталізатором в реакціях фотоокиснення в водному середовищі органічних барвників ультрафіолетовим випромінюванням. Фотокаталітична активність синтезованого рутильного TiO_2 визначалася при руйнуванні розчиненого у водному середовищі барвника Конго червоного (КЧ). Ефективність TiO_2 вивчали шляхом дослідження впливу кількості TiO_2 та концентрації H_2O_2. Встановлено, що повне знебарвлення барвника досягається всього за 10 хвилин УФ-опромінення, за умов концентрація фотокаталізатора 1.5 г/л, концентрація H_2O_2 5 мМ і початкової концентрації барвника КЧ 5 мг/л, при швидкості розкладу 2.1959 $хв^{-1}$.

Ключові слова: титан (IV) оксид; рутил; Конго червоний; фотокаталізатор.